https://doi.org/10.3311/PPci.21028

Periodica Polytechnica Civil Engineering, 67(1), pp. 211–223, 2023

Analytical GNI Analysis for Lateral-torsional Behavior of Thin-walled Beams with Doubly-symmetric I-Sections

Muhammad Z. Haffar[1], Martin Horáček[2], Sándor Ádány[1*]

[1] Department of Structural Mechanics, Faculty of Civil Engineering, Budapest University of Technology and Economics, H-1111 Budapest, Műegyetem rkp. 3., Hungary
[2] Institute of Metal and Timber Structures, Faculty of Civil Engineering, Brno University of Technology, Veveří 331/95, 602 00 Brno, Czech Republic
[*] Corresponding author, e-mail: adany.sandor@emk.bme.hu

Received: 18 August 2022, Accepted: 12 October 2022, Published online: 22 November 2022

Abstract

In this paper elastic lateral-torsional behavior of simple beams is discussed. The motivation of the presented research is the observation that classic analytical prediction and finite element prediction are, typically, considerably different, when the second-order nonlinear behavior of beams with initial imperfections is analyzed. In order to understand and explain the observed differences, a novel analytical solution is presented for the geometrically nonlinear analysis of beams with initial geometric imperfection. The presented analytical solution is derived for doubly-symmetric cross-sections, but with the novelty that it takes into consideration the changing geometry as the load is increasing. The most important steps of the derivations are summarized, and the resulted formulae are briefly discussed. Numerical studies are performed, too: the results of the new analytical formulae are compared to those from shell finite element analysis. The results suggest that the new formulae are able to capture the most important elements of the behavior. By the analytical and numerical results, it is proved that classic analytical solutions for the geometrically nonlinear analysis of beams with geometric imperfections are necessarily different from the numerical results obtained by incremental-iterative procedures.

Keywords

lateral-torsional buckling, geometrically nonlinear analysis, geometric imperfections

1 Introduction

Buckling is one of the most critical behavior and failure types of thin-walled members. In the case of beams, when the primary action is bending, the global buckling is usually called *lateral-torsional buckling*, popularly abbreviated as LTB. If the beam is subjected to a loading with increasing intensity, the displacements are slowly increasing in the plane of the loading, but when the load approximates a certain level, the member can start to develop rapidly increasing out-of-plane displacements characterized by twisting rotations and translations perpendicular to the plane of loading. In a general sense this phenomenon is called *buckling*. If the beam is free from imperfections and its material is perfectly elastic, the analysis is usually termed as *linear buckling analysis* (LBA). The LTB problem, mathematically, is a generalized eigen-value problem: the eigen-vectors (or eigen-functions) are the *buckling shapes*, the eigen-values are the critical values of the load, e.g., *critical moments*. Closed-form analytical solutions for the critical moments are known, at least for simpler cases, and can be found in classic textbooks [1, 2]. It must be noted, however, that when the cross-section, or loading, or boundary conditions of the beam are less regular, it is not easy to find analytical solutions, that is why researches on LTB LBA continued for decades, see e.g., [3], and even nowadays the topic shows up in research papers [4–7].

Practical structures are never perfect, and in the case of buckling the – even small – initial imperfections can significantly influence the behavior. That is why the solution of the LBA problem alone is usually not sufficient to predict the capacity, but somehow the effect of imperfections must be included. One of the simplest ways to consider the imperfections is to use (equivalent) geometric imperfections, i.e., to consider that the beam is not perfectly straight even before it is loaded. The concept, probably, was first applied by Young [8] for columns, and then was extended to other types of buckling.

Cite this article as: Haffar, M. Z., Horáček, M., Ádány, S. "Analytical GNI Analysis for Lateral-torsional Behavior of Thin-walled Beams with Doubly-symmetric I-Sections", Periodica Polytechnica Civil Engineering, 67(1), pp. 211–223, 2023. https://doi.org/10.3311/PPci.21028

It was realized very early that applying an initial imperfection can be a useful tool in predicting the load-bearing capacity. The approach, perhaps, was first applied in [9], and the approach and resulting formula are named after the authors: Ayrton-Perry approach/formula. This approach, indeed, is the basis of the European buckling curves, proposed by [10], which are still in use in the current Eurocode standards, e.g., [11, 12], both for column buckling and LTB. Further generalized application of the approach is possible, as proposed e.g., in [13].

Since nowadays structural analysis is typically performed by computer programs, most popularly by the finite element method (FEM), it is a possible design approach to directly consider geometric imperfections in the analysis. If the analysis is elastic, it is typically abbreviated as GNIA (i.e., *Geometrically Non-linear Analysis with Imperfections*), and this approach is directly included in many design standards, including [11]. Even so, it is not necessarily evident what shape and magnitude of geometric imperfections should be applied. A popular idea is to apply some buckling shape, i.e., the result of an LBA analysis, but the question has not been fully solved yet, which explains the more recent research effort on this topic, e.g., [14].

Recently it was shown in [15], however, that there is a discrepancy between the results predicted by the classic analytical GNI solution (see e.g., [14, 16] and those calculated by shell FEM GNI analyses. The discrepancies can be important. Also, the discrepancies are not limited to the difference of certain numerical values, but some basic features of the behavior are affected. For example, while the classic analytical solutions predict symmetric bifurcation for LTB, independently of the cross-section, shell finite element GNI analysis suggests asymmetric bifurcation in some cases. Moreover, while the classic analytical solutions predict that the maximal moment equals the critical moment, numerical results do not always confirm this prediction. To reveal the reasons of the experienced discrepancies, the authors developed an advanced analytical model.

The primary aim of this paper, therefore, is to present an advanced analytical solution for the nonlinear behavior of simple beams with initial geometric imperfections. Some preliminary results have been reported in [17]. In this paper a more comprehensive presentation and discussion of the developed advanced analytical models are included, focusing on doubly-symmetric cross-sections. (It is to note that more general cross-sections will be discussed in a separate paper.)

In the paper, first the proposed analytical model is summarized, then solutions are presented to various problems, starting with brief mentioning of classic solutions (LBA and GNIA), then presenting the most advanced one when the load is applied in increments and during the incremental procedure the stiffness matrix and load vectors are updated. Numerical studies have also been conducted, the results of which are summarized at the end of the paper. Finally, conclusions are drawn.

2 General description of the analytical model

In this section the applied analytical model is described. The model is developed for simply-supported beams subjected to two opposite end-moments, resulting in the uniform moment along the length, see Fig. 1. The cross-section is doubly-symmetric. In the examples I-sections beams are considered, being the most typical steel beams, but the derivation is valid for any doubly-symmetric cross-section.

Depending on the purpose of the analysis (e.g., linear buckling analysis, first- or second-order static analysis) the model needs adjustments, as we will see in subsequent Sections; here a generic description is given.

The mechanical features are as follows: (i) the thin-walled member is modelled as an assembly of plane plates (referred to also as strips), (ii) global buckling/behavior is defined as the modes with no cross-section distortion, and with no in-plane transverse extension and no in-plane shear deformations, (iii) the stress-strain field is assumed according to Kirchhoff plate theory for the out-of-plane behavior and to a conventional 2D stress-strain state for the in-plane behavior of each plate element, (iv) the material model follows Hooke's law, (v) the end moments are applied as distributed loading, linearly varying over the (end) cross-sections.

Since global behavior is defined as displacements with no cross-section distortion, the global displacements of the reference line of the member (defined by the cross-section mass centers) are expressed as follows:

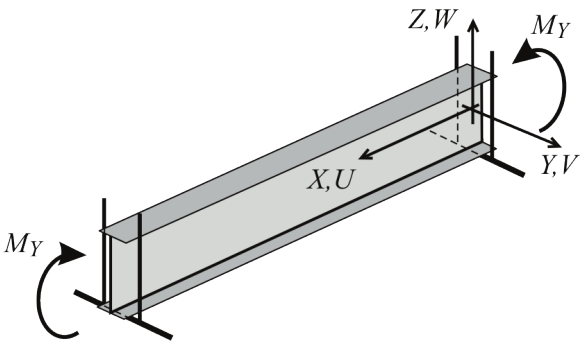

Fig. 1 Simply supported beam in uniform bending

$$\begin{aligned} U &= U_m f_U(X), \\ V &= V_m f_V(X), \\ W &= W_m f_W(X), \\ \varnothing &= \varnothing_m f_\varnothing(X), \end{aligned} \tag{1}$$

where U_m, V_m and W_m are global translational displacement amplitudes, $\varnothing_m$ is the global torsional displacement amplitude, and the f functions determine the longitudinal distributions. Though the longitudinal displacements may have some effect, this effect is typically negligible for practical cross-sections and practical length ranges, therefore, the global longitudinal displacement of the cross-sections will be neglected here, i.e., $U_m = 0$ is assumed.

From the global displacements of the cross-section the displacements of the strips' (longitudinal) mid-lines can be defined as follows (see Fig. 2):

$$v_{m,i} = V\cos\alpha_i + W\sin\alpha_i + \varnothing\left(Y_{m,i}\sin\alpha_i - Z_{m,i}\cos\alpha_i\right), \tag{2}$$

$$w_{m,i} = -V\sin\alpha_i + W\cos\alpha_i + \varnothing\left(Y_{m,i}\cos\alpha_i + Z_{m,i}\sin\alpha_i\right), \tag{3}$$

$$\varphi_{m,i} = \varnothing, \tag{4}$$

$$u_{m,i} = -\frac{\partial V}{\partial X}Y_{m,i} - \frac{\partial W}{\partial X}Z_{m,i} + \frac{\partial \varnothing}{\partial X}\omega_{m,i}, \tag{5}$$

where $Y_{m,i}$ and $Z_{m,i}$ are the global coordinates of the i-th strip's mid-point, $\omega_{m,i}$ is the sectoral coordinate introduced by Vlasov [2] (with respect to shear center) at the location of the i-th strip mid-point. All the mid-point displacements are expressed in terms of the global longitudinal coordinate X. Moreover, the local x and global X longitudinal axis are parallel, and the X and x coordinates are numerically identical. Note that formulae for the calculation of shear center and sectoral coordinates can be found in textbooks, as well as a good summary is given in the Eurocode for cold-formed steel, see Annex C of [12].

By using the above displacements in the mid-point of the strips, the local displacement functions of the strips can be expressed as follows:

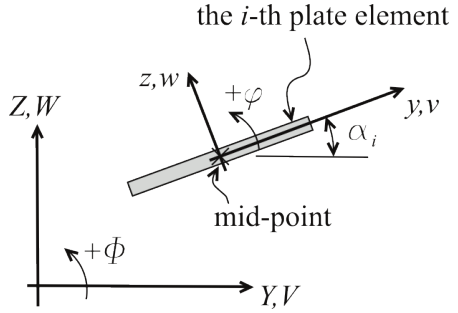

Fig. 2 Global/local coordinates and displacements

$$u_i = u_{m,i} - v_{m,i}y - w_{m,i}z - \varphi_{m,i}yz, \tag{6}$$

$$v_i = v_{m,i} - \varphi_{m,i}z, \tag{7}$$

$$w_i = w_{m,i} + \varphi_{m,i}y, \tag{8}$$

$$\varphi_i = \varphi_{m,i}. \tag{9}$$

Thus, the $u(x, y, z)$, $v(x, y, z)$, $w(x, y)$ and (x) local displacement functions of each strip are expressed by the U_m, V_m and W_m global displacement amplitudes.

For the solution the energy method is applied, i.e., the equilibrium is interpreted as the stationary point of the total potential function. The internal potential (i.e., accumulated elastic strain energy) and external potential (i.e., the negative of the work done by the loads) should be expressed. Classical formulae are used. The strain energy is expressed as follows:

$$\Pi_{int} = \frac{1}{2}\sum_{i=1}^{n}\int_V Et_i\left(\frac{\partial u_i}{\partial x}\right)^2 + \frac{Et_i^3}{12}\left(\frac{\partial^2 w_i}{\partial x^2}\right)^2 + \frac{Gt_i^3}{3}\left(\frac{\partial^2 w_i}{\partial x \partial y}\right)^2 \mathrm{dA}, \tag{10}$$

where the integral, in fact, means double integration with respect to x and y, for the whole surface of the strip, i.e., x is taken from 0 to L, and y is taken from $(-b_i/2)$ to $(+b_i/2)$. Moreover, L is the member length, bi and ti are the width and thickness of the i-th strip, respectively, n is the number of strips, and E and G are Young's modulus and shear modulus, respectively. It is to observe that the first term within the integral represents the membrane effect, while the second and third terms represent plate flexure.

The external potential is the negative of the work done by the external loads, and expressed as follows:

$$\Pi_{ext} = -\sum_{i=1}^{n}\int_V \sigma_{x,i}\varepsilon_{x,i}\mathrm{dA}. \tag{11}$$

In this expression $\sigma_{x,i}$ is the longitudinal normal stress function for the i-th strip, $\varepsilon_{x,i}$ is the corresponding strain function (i.e., longitudinal normal strain). Depending on the problem we want to solve, sometimes the first-order (linear) strain is needed, sometimes the non-linear strain, while in other cases both. For the linear part:

$$\varepsilon_{x,i}^{I} = \frac{\partial u_i}{\partial x}. \tag{12}$$

For the non-linear part we use the Green-Lagrange strain tensor, the strains can be expressed as:

$$\varepsilon_{x,i}^{II} = \frac{1}{2}\left[\left(\frac{\partial v_i}{\partial x}\right)^2 + \left(\frac{\partial w_i}{\partial x}\right)^2\right]. \tag{13}$$

It is to observe that the second-order strain can readily be interpreted as the quadratic approximation of the longitudinal elongation/shortening due to the inclination of the fibers of the strip, which inclination is nothing else than the first derivative of the v and w transverse translation functions with respect to x.

The stress in the member, therefore the stress in each strip, is dependent on the loading, as well as on whether we consider the changed stress state as the member deforms. If the member is subjected to uniaxial bending, the primary, first-order stress is linearly varying with Z, and can be expressed as:

$$\sigma_{x,i}^{I} = -\frac{M_Y}{I_y}\left(Z_{m,i} + y \times sin(\alpha_i) + z \times cos(\alpha_i)\right), \tag{14}$$

where I_y is the second moment of area calculated for the Y-axis. Note that later on we will consider second-order stress terms, too.

Once the total potential is expressed, we can use the theorem of stationarity of total potential to find equilibrium. Practically, the first partial derivatives with respect to the displacement parameters (namely: U_m, V_m and W_m) must be equal to zero. This leads to a system of equations. The nature of this equation system is dependent on what stress and strain terms we include in calculating the total potential, as will be shown as follows.

3 Classic analytical solution: linear buckling analysis

To get the linear buckling problem (LBA), we need to consider trigonometric global displacement functions. When the member is hinged (i.e., forked), single half sine-waves work well, the considered displacement functions are, therefore:

$$\begin{aligned} V &= V_m sin\frac{\pi X}{L}, \\ W &= W_m sin\frac{\pi X}{L}, \\ \varnothing &= \varnothing_m sin\frac{\pi X}{L}, \end{aligned} \tag{15}$$

where W_m, V_m and $\varnothing_m$ are the amplitudes for the vertical and lateral translations and for the twisting rotation, respectively, X is the longitudinal coordinate axis, and L is the beam length. By following the procedure described above, the theorem of stationarity of potential leads to a system of linear equations, which, in other words, is a generalized eigen-value problem. This reads as:

$$\begin{bmatrix} F_y & 0 & 0 \\ 0 & F_z & 0 \\ 0 & 0 & F_x \end{bmatrix} . \begin{bmatrix} W_m \\ V_m \\ \varnothing_m \end{bmatrix} + \begin{bmatrix} 0 & 0 & 0 \\ 0 & 0 & M_Y \\ 0 & M_Y & 0 \end{bmatrix} . \begin{bmatrix} W_m \\ V_m \\ \varnothing_m \end{bmatrix} = \begin{bmatrix} 0 \\ 0 \\ 0 \end{bmatrix}, \tag{16}$$

where the F_x, F_y and F_z symbols are defined as follows:

$$F_y = \frac{\pi^2 EI_y}{L^2}, F_z = \frac{\pi^2 EI_z}{L^2}, F_x = F_t + F_w = GI_t + \frac{\pi^2 EI_w}{L^2}, \tag{17}$$

where I_y and I_z are the second moments of areas calculated for the Y-axis and Z-axis, respectively, I_w is the warping constant, I_t is the torsion constant. The first matrix is the $\boldsymbol{K}_e$ elastic stiffness matrix, while the second one is the $\boldsymbol{K}_g$ geometric stiffness matrix of the problem. The first equation is independent of the other two equations, can be solved separately, and lead to the solution that $W_m = 0$. This means that in order to get a buckling solution, displacement in the plane of the bending is not necessary to consider. The second and third equation form a generalized eigen-value problem. Due to its simplicity, there is analytical solution, which is nothing else than the critical moment value (s):

$$M_{cr} = \pm\sqrt{F_x F_z}\ . \tag{18}$$

Since the cross-section is doubly-symmetric, the two algebraic solutions are plus-minus pair. The physical meaning is that if there is a positive critical moment with, say, the top flange compressed, then there is another critical moment with the same magnitude with the opposite, say, bottom flange compressed. By back-substitution, we can find the buckled shape. Longitudinally, both V and $\varnothing$ have half-sine-wave shape. Since $\boldsymbol{K} + \boldsymbol{K}_g$ is rank-deficient, the V_m and $\varnothing_m$ amplitudes are dependent on each other, otherwise the amplitudes are arbitrary. The relationship between V_m and $\varnothing_m$ is as follows:

$$V_m = -\varnothing_m \frac{M_{cr}}{F_z}\ . \tag{19}$$

4 Classic analytical solution: GNIA

Next, let us briefly consider geometrically nonlinear analysis with geometric imperfection. The above derivation can similarly be completed by considering a geometric imperfection in the form of the buckling shape. The details of the derivation for this classic case are not shown. The derivation leads to an equation similar to Eq. (16), but the right-hand side will not be zero anymore, and, based on the observation from LBA we can simply eliminate the displacement in the plane of the bending. Finally, there are two equations, which can be written as follows:

$$\begin{bmatrix} F_z & 0 \\ 0 & F_x \end{bmatrix} \cdot \begin{bmatrix} \Delta V_m \\ \Delta \varnothing_m \end{bmatrix} + \begin{bmatrix} 0 & M_Y \\ M_Y & 0 \end{bmatrix} \cdot \begin{bmatrix} \Delta V_m \\ \Delta \varnothing_m \end{bmatrix} = \begin{bmatrix} -M_y \varnothing_{m,ini} \\ -M_y V_{m,ini} \end{bmatrix}, \tag{20}$$

It is to emphasize that in the above equation $V_{m,ini}$ and $\varnothing_{m,ini}$ are the amplitudes of the initial geometry (when the beam is not loaded yet), and ΔV_m and $\Delta\varnothing_m$ represent the displacement increment from the imperfect state. The right-hand-side vector is non-zero, and this can conveniently be called as load vector, which depends on the amplitudes of the initial imperfect geometry. The equation system can be solved, and unique solution can be found, as follows:

$$\Delta V_m = V_{m,ini} \frac{1}{M_{cr} / M_Y - 1}, \Delta\varnothing_m = \varnothing_{m,ini} \frac{1}{M_{cr} / M_Y - 1}. \tag{21}$$

The total displacement is the sum of the initial one and the increment, which finally leads to the well-known formulae expressing the displacement amplification:

$$\Delta V_m + V_{m,ini} = V_{m,ini} \frac{1}{1 - M_Y / M_{cr}}, \tag{22}$$

$$\Delta\varnothing_m + \varnothing_{m,ini} = \varnothing_{m,ini} \frac{1}{1 - M_Y / M_{cr}}. \tag{23}$$

The above formulae are also known (and will be referred to) as Young's formula. The formula is widely used in design practice (encouraged by many design codes, too) to estimate the amplification due to second-order effects.

5 Classic GNIA with load increments

Now let us repeat the classical GNI analysis, but with incremental loading. The same analytical model is employed as above, however, with some modifications. First, the primary and secondary displacements are not separated, i.e., the vertical translations will be considered, too. Since the primary displacements are essentially due to the primary loading, which is a uniform moment, a quadratic function is assumed for *W*, in accordance with the classic first-order solution. Therefore, the assumed global displacement functions are:

$$\begin{aligned} W &= W_m \frac{4}{L^2}(L - X)X, \\ V &= V_m \sin\left(\frac{\pi X}{L}\right), \\ \varnothing &= \varnothing_m \sin\left(\frac{\pi X}{L}\right). \end{aligned} \tag{24}$$

It is highlighted that *V*, *W* and $\varnothing$ are the total displacements, measured from the perfect member.

Another small modification is that we assume arbitrary initial amplitudes, which means that the initial shape is not necessarily identical to a buckling shape. (But we will consider this special case, too.)

$$V_{ini} = V_{m,ini} \sin\left(\frac{\pi X}{L}\right), \ \varnothing_{ini} = \varnothing_{m,ini} \sin\left(\frac{\pi X}{L}\right) \tag{25}$$

Finally, which is the most important modification, the load is applied in increments. After a certain number of increments the load value is M_{Ya}, and the corresponding displacement amplitudes are: W_{ma}, V_{ma} and $\varnothing_{ma}$. This state is an equilibrium state and is referred to as state 'a'. The goal is to find the displacement increments ΔW_{ma}, ΔV_{ma} and $\Delta\varnothing_{ma}$, as the load is further increased by ΔM_y, that is when the member reaches the next equilibrium state, referred to as state 'b'. The load and the displacements at the end of the incremental step are, therefore:

$$\begin{aligned} &M_{Yb} = M_{Ya} + \Delta M_Y \ W_{mb} = W_{ma} + \Delta W_m, \\ &V_{mb} = V_{ma} + \Delta V_m \ \varnothing_{mb} = \varnothing_{ma} + \Delta\varnothing_m. \end{aligned} \tag{26}$$

The incremental load application initiates some modification in the derivations, summarized as follows. When constructing the potential function, we need the increment of the internal potential, that is the increment of the strain energy as the member deforms from state 'a' to state 'b'. In each state the accumulated strain energy can be expressed by directly substituting into Eq. (10) the displacement parameters, hence the increment can readily be expressed as the difference between the strain energies at the two states.

$$\Delta\Pi_{int} = \Pi_{int,b} - \Pi_{int,a}, \tag{27}$$

with

$$\begin{aligned} \Pi_{int,a} = \frac{1}{2} \sum_{i=1}^{n} \int_V & Et_i \left(\frac{\partial u_{ia}}{\partial x}\right)^2 + \frac{Et_i^3}{12} \left(\frac{\partial^2 w_{ia}}{\partial x^2}\right)^2 \\ & + \frac{Gt_i^3}{3} \left(\frac{\partial^2 w_{ia}}{\partial x \partial y}\right)^2 dA, \end{aligned} \tag{28}$$

$$\begin{aligned} \Pi_{int,b} = \frac{1}{2} \sum_{i=1}^{n} \int_V & Et_i \left(\frac{\partial u_{ib}}{\partial x}\right)^2 + \frac{Et_i^3}{12} \left(\frac{\partial^2 w_{ib}}{\partial x^2}\right)^2 \\ & + \frac{Gt_i^3}{3} \left(\frac{\partial^2 w_{ib}}{\partial x \partial y}\right)^2 dA. \end{aligned} \tag{29}$$

Hence, the strain energy increment is expressed with respect to the displacement increments ΔW_m, ΔV_m and $\Delta\varnothing_m$.

The external part of the total potential can be handled similarly. This part of the potential increment is the negative of the work done by the stresses on the strain increments, where the strain is the sum of the first-order and the second-order strain. The increment of the first-order part can directly be calculated from Eq. (12), but applying it to the displacement increment:

$$\Delta\varepsilon_{x,i}{}^{I} = \frac{\partial \Delta u_i}{\partial x}. \tag{30}$$

For the second-order strain increment we apply Eq. (13), as follows:

$$\Delta\varepsilon_{x,i}{}^{II} = \frac{1}{2}\left[\left(\frac{\partial(v_{ia}+\Delta v_i)}{\partial x}\right)^2 - \left(\frac{\partial v_{ia}}{\partial x}\right)^2 + \left(\frac{\partial(w_{ia}+\Delta w_i)}{\partial x}\right)^2 - \left(\frac{\partial w_{ia}}{\partial x}\right)^2\right], \tag{31}$$

from which:

$$\Delta\varepsilon_{x,i}{}^{II} = \frac{1}{2}\left(\frac{\partial \Delta v_i}{\partial x}\right)^2 + \frac{\partial \Delta v_i}{\partial x}\frac{\partial v_{ia}}{\partial x} + \frac{1}{2}\left(\frac{\partial \Delta w_i}{\partial x}\right)^2 + \frac{\partial \Delta w_i}{\partial x}\frac{\partial w_{ia}}{\partial x}. \tag{32}$$

As far as stresses are concerned, obviously we have the primary stress, therefore we apply Eq. (14).

$$\sigma_{x,ib}{}^{I} = -\frac{M_{Ya}+\Delta M_Y}{I_y}\left(Z_{m,i} + y\times sin(\alpha_i) + z\times cos(\alpha_i)\right) \tag{33}$$

Thus, with all the above considerations, the expression for the increment of the external potential is as follows:

$$\Delta\Pi_{ext} = -\sum_{i=1}^{n}\int_V \left(\sigma_{x,ib}{}^{I}\right)\left(\Delta\varepsilon_{x,i}{}^{I} + \Delta\varepsilon_{x,i}{}^{II}\right)\mathrm{dV}. \tag{34}$$

It is to observe that this work increment, again, is expressed with respect to the displacement increments ΔV_m, ΔW_m and $\Delta\varnothing_m$, hence the increment of the total potential is expressed by the displacement increments.

In equilibrium the total potential is stationary, therefore:

$$\frac{\partial\Delta\Pi}{\partial\Delta W_m} = 0 \quad \frac{\partial\Delta\Pi}{\partial\Delta V_m} = 0 \quad \frac{\partial\Delta\Pi}{\partial\Delta\varnothing_m} = 0, \tag{35}$$

with $\Delta\Pi = \Delta\Pi_{int} + \Delta\Pi_{ext}$.

Eq. (35) is a system of three equations, which can be summarized in one single matrix equation as follows:

$$\boldsymbol{K}_e\Delta\boldsymbol{d} + M_{Yb}\boldsymbol{K}_g\Delta\boldsymbol{d} = \Delta\boldsymbol{f}, \tag{36}$$

where

$$\boldsymbol{K}_e = \begin{bmatrix} F_y\frac{64}{\pi^2 L} & 0 & 0 \\ 0 & F_z\frac{\pi^2}{2L} & 0 \\ 0 & 0 & F_x\frac{\pi^2}{2L} \end{bmatrix} \quad \boldsymbol{K}_g = \begin{bmatrix} 0 & 0 & 0 \\ 0 & 0 & \frac{\pi^2}{2L} \\ 0 & \frac{\pi^2}{2L} & 0 \end{bmatrix}, \tag{37}$$

$$\Delta\boldsymbol{d} = \begin{bmatrix} \Delta W_m \\ \Delta V_m \\ \Delta\varnothing_m \end{bmatrix} \quad \Delta\boldsymbol{f} = \begin{bmatrix} -M_{Yb}\frac{8}{L} - W_{ma}F_y\frac{64}{\pi^2 L} \\ -M_{Yb}\varnothing_{ma}\frac{\pi^2}{2L} - \left(V_{ma}-V_{m,ini}\right)F_z\frac{\pi^2}{2L} \\ -M_{Yb}V_{ma}\frac{\pi^2}{2L} - \left(\varnothing_{ma}-\varnothing_{m,ini}\right)F_x\frac{\pi^2}{2L} \end{bmatrix}$$

The above equation system can be solved analytically. The solution is as follows:

$$\Delta W_m = -M_{yb}\frac{\pi^2}{8F_y} - W_{ma}, \tag{38}$$

$$\Delta V_m = \frac{V_{m,ini}\frac{M_{cr}{}^2}{M_{Yb}{}^2} - \varnothing_{m,ini}\frac{F_x}{M_{yb}}}{\frac{M_{cr}{}^2}{M_{Yb}{}^2} - 1} - V_{ma}, \tag{39}$$

$$\Delta\varnothing_m = \frac{-V_{m,ini}\frac{F_z}{M_{Yb}} + \varnothing_{m,ini}\frac{M_{cr}{}^2}{M_{yb}{}^2}}{\frac{M_{cr}{}^2}{M_{Yb}{}^2} - 1} - \varnothing_{ma}. \tag{40}$$

From the above formulae it is clear that the primary (vertical) displacement is independent of the other displacements and vice-versa. It is also noteworthy that even if we consider only one component of the initial imperfection, i.e., if we consider either initial lateral translation or initial twisting rotation, still there is non-zero increment of both. In other words: lateral displacement induces twisting rotation, and twisting rotation induces lateral translation. This also means that typically the amplification of V_{mv} and $\varnothing_m$ are different, i.e., the shape of the beam changes during the loading process (and not only the initial shape is amplified).

Let us see the specific case when the initial shape is a buckling shape. We can consider the relationship between the lateral translation and twisting rotation amplitude, as in Eq. (19). Moreover, for the sake of simplicity, let us focus on the first incremental step, i.e.: $W_{ma} = 0$, $V_{ma} = V_{m,ini}$, $\varnothing_{ma} = \varnothing_{m,ini}$, and also $M_{Ya} = 0$, therefore $M_{Yb} = \Delta M_Y$. The above formulae are significantly simplified, and read as follows:

$$\Delta W_m = -M_{Yb}\frac{\pi^2}{8F_y}, \tag{41}$$

$$\Delta V_m = V_{m,ini}\frac{1}{M_{cr}/M_{Yb}-1}, \tag{42}$$

$$\Delta \varnothing_m = \varnothing_{m,ini}\frac{1}{M_{cr}/M_{Yb}-1}, \tag{43}$$

from which the total displacements at the end of this load step are:

$$W_{mb} = -M_{Yb}\frac{\pi^2}{8F_y}, \tag{44}$$

$$V_{mb} = \Delta V_m + V_{m,ini} = V_{m,ini}\frac{1}{1-M_{Yb}/M_{cr}}, \tag{45}$$

$$\varnothing_{mb} = \Delta\varnothing_m + \varnothing_{m,ini} = \varnothing_{m,ini}\frac{1}{1-M_{Yb}/M_{cr}}. \tag{46}$$

The obvious observation is that we get back the classic analytical solutions, even if the load is applied in increments. This is true for the vertical translation (classic first-order solution) and the other displacements (classic GNIA solution). Another important observation is that the initial translation and initial twisting are identically amplified; the consequence is that once the initial geometry is the buckled shape, the lateral translation and twisting rotation remains similar to the buckling shape throughout the loading process. As we will see in the next section, this is the consequence of the fact that the stiffness matrix is unchanged during the analysis, see Eq. (37). In other words, in this model $\boldsymbol{K}_g$ is not updated.

6 GNIA with updated stiffness

In this section we perform GNIA similar to that in the previous section, however, the stiffness matrix and load vector are updated in each incremental step, in order to follow the typical scenario in an incremental finite element analysis.

The same displacement functions and same initial geometry are used as above, see Eqs. (24–25). The strain energy is calculated as in the previous section, see Eqs. (27–29). Moreover, the first- and second-order strains are calculated as previously, see Eqs. (30) and (32). The important difference here is that the stresses need to be determined in each load step, and the external potential, therefore, is calculated differently.

We have the primary stress, just as expressed by Eq. (33). However, as now the load is imposed on the member by increments, and in each increment, we calculate the actual displacements, second-order stresses develop due to the displacements, namely: due to V and $\varnothing$. To determine these second-order stresses, we utilize classic differential equations, namely equations (6–5) and (6–6) of [1].

Equation (6–5) of [1] can be written (by using the notations of the actual paper) as follows:

$$EI_z\frac{\partial^2 V}{\partial X^2} - \varnothing M_Y = 0. \tag{47}$$

This equation expresses the moment equilibrium in the minor-axis direction. The first term represents the stress resultant, which, if initial geometric imperfection is present, is to be calculated from the $(V - V_{ini})$ displacement. The second term represents the minor-axis component of the M_Y as the cross-section is twisted. Since the resultant of the stresses for the minor-axis bending can be expressed as:

$$M_Z = EI_z\frac{\partial^2\left(V - V_{ini}\right)}{\partial X^2}, \tag{48}$$

the minor-axis bending moment due to twisting rotation of the cross-section is:

$$M_Z = M_Y\varnothing, \tag{49}$$

from which the stress in the i-th strip, e.g., at state 'b', is:

$$\sigma_{x,ib}{}^{II,\varnothing} = -\frac{M_{Yb}\varnothing_{ma}}{I_z}\left(Y_{m,i} + y\times\cos\left(\alpha_i\right) + z\times\sin\left(\alpha_i\right)\right)\sin\left(\frac{\pi X}{L}\right). \tag{50}$$

Thus, when the member is twisted, M_Y generates M_Z. This can readily be illustrated, see Fig. 3. It is to note that the assumed longitudinal distribution of $\varnothing$ is a half-sine wave, accordingly the longitudinal distribution of M_Z is a half sine-wave, which is different from the uniform longitudinal distribution of M_Y.

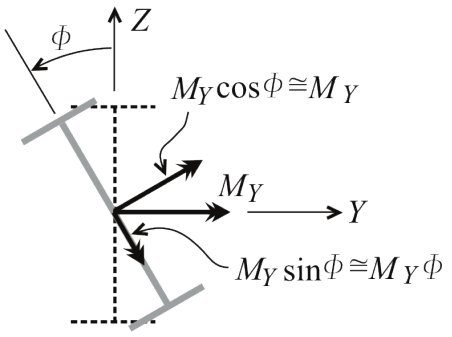

Fig. 3 Illustration of minor-axis moment induced by twist

Similarly, if the member is laterally displaced, M_Y generates bi-moment. Equation (6–6) of [1] can be written (by using the notations of the actual paper) as:w

$$GI_t \frac{\partial \varnothing}{\partial X} - EI_w \frac{\partial^3 \varnothing}{\partial X^3} + \frac{\partial V}{\partial X} M_Y = 0\,. \tag{51}$$

This equation expresses the equilibrium of torsional moments. The first and second terms represent the stress resultants from Saint-Venant torsion (i.e., resultants of shear stresses) and warping torsion (i.e., resultant of warping normal stresses). If initial geometric imperfection is present, these terms should be calculated from the ($\varnothing - \varnothing_{ini}$) displacement. The third term represents the torsional moment component of the external M_Y moment, due to the inclination of the cross-section as it laterally displaces. The actual version of Eq. (51), therefore, can be written as follows:

$$GI_t \frac{\partial\left(\varnothing - \varnothing_{ini}\right)}{\partial X} - EI_w \frac{\partial^3\left(\varnothing - \varnothing_{ini}\right)}{\partial X^3} + \frac{\partial V}{\partial X} M_Y = 0\,. \tag{52}$$

Both V and $\varnothing$ are assumed to have a half sine-wave longitudinally, and the same for the initial shapes. By considering these functions we get:

$$GI_t \frac{\pi}{L}\left(\varnothing_m - \varnothing_{m,ini}\right) + EI_w \frac{\pi^3}{L^3}\left(\varnothing_m - \varnothing_{m,ini}\right) + M_Y \frac{\pi}{L} V_m = 0, \tag{53}$$

$$\left(\varnothing_m - \varnothing_{m,ini}\right) = \frac{-M_Y V_m}{EI_w \frac{\pi^2}{L^2} + GI_t} = \frac{-M_Y V_m}{F_w + F_t}\,. \tag{54}$$

It is known that the torsional resultant of the warping normal stresses is the bi-moment:

$$B = EI_w \frac{\partial^2\left(\varnothing - \varnothing_{ini}\right)}{\partial X^2}\,, \tag{55}$$

from which, by using Eqs. (24–25), the bi-moment amplitude can be expressed as:

$$B_m = -EI_w \frac{\pi^2}{L^2}\left(\varnothing_m - \varnothing_{m,ini}\right) = -F_w\left(\varnothing_m - \varnothing_{m,ini}\right). \tag{56}$$

Substituting Eq. (54) into Eq. (56) we get the bi-moment amplitude which represents the influence of the lateral translation, as follows:

$$B_m = F_w \frac{M_Y V_m}{F_w + F_t} = M_Y V_m \frac{1}{1 + F_t / F_w} \tag{57}$$

From the bi-moment the stress in the i-th strip can readily be calculated, e.g., at state 'b' it is:

$$\sigma_{x,ib}{}^{II,V} = -\frac{M_{Yb} V_{ma}}{I_w} \frac{1}{1 + F_t / F_w} \omega_i\left(y,z\right) \sin\left(\frac{\pi X}{L}\right), \tag{58}$$

where ω_i is the sectoral coordinate function for the i-th strip.

In the case of a doubly-symmetric I-section beam, the normal stresses due to lateral displacement can be illustrated as in Fig. 4, where the equilibrium of a part of the beam is presented.

As it is shown in Fig. 4, the top flange is subjected to uniform compression at the supports, the bottom flange is to uniform tension. Between the supports the flanges are subjected to eccentric compression/tension, therefore there is lateral bending from which linearly varying stresses develop, just as if the cross-section were subjected to bi-moment. (It is to mention, however, that this illustration considers the normal stresses only. Shear stresses must also be involved in order to maintain torsional equilibrium.)

Thus, with all the above considerations, the external potential increment in Eq. (34) must be supplemented by an additional term, and finally the external work increment is expressed as follows:

$$\begin{aligned}\Delta\Pi_{ext} = &-\sum_{i=1}^{n}\int_V \left(\sigma_{x,ib}{}^{I}\right)\left(\Delta\varepsilon_{x,i}{}^{I} + \Delta\varepsilon_{x,i}{}^{II}\right)\mathrm{dA} - \\ &-\sum_{i=1}^{n}\int_V \left(\sigma_{x,ib}{}^{II,\varnothing} + \sigma_{x,ib}{}^{II,V}\right)\left(\Delta\varepsilon_{x,i}{}^{II}\right)\mathrm{dA}.\end{aligned} \tag{59}$$

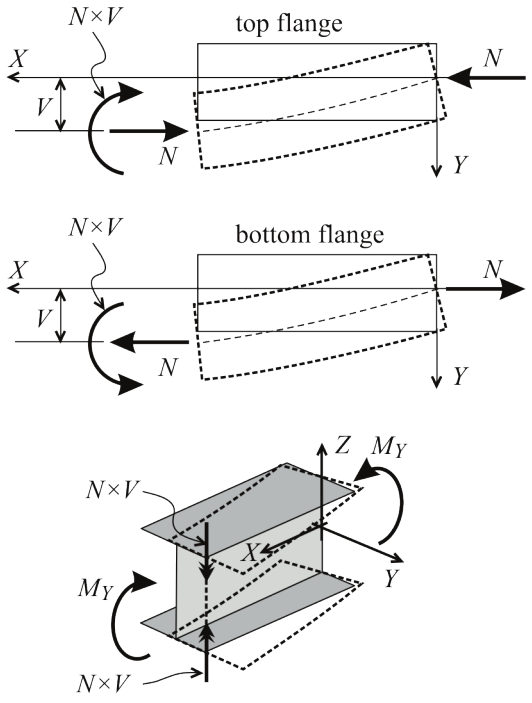

Fig. 4 Illustration of bi-moment induced by lateral translation

In equilibrium the total potential is stationary, therefore, we apply Eq. (35), which leads to a system of equations just as Eq. (36), however, now and are slightly different, as follows:

$$\boldsymbol{K}_g = \begin{bmatrix} 0 & 0 & -\varnothing_{ma}\dfrac{2}{L} \\ 0 & 0 & \dfrac{\pi^2}{2L} \\ -\varnothing_{ma}\dfrac{2}{L} & \dfrac{\pi^2}{2L} & 0 \end{bmatrix} \tag{60}$$

$$\Delta \boldsymbol{f} = \begin{bmatrix} -M_{Yb}\dfrac{8}{L} + M_{Yb}\varnothing_{ma}^2\dfrac{2}{L} - W_{ma}F_y\dfrac{64}{\pi^2 L} \\ -M_{Yb}\varnothing_{ma}\dfrac{\pi^2}{2L} - \left(V_{ma} - V_{m,ini}\right)F_z\dfrac{\pi^2}{2L} \\ -M_{Yb}V_{ma}\dfrac{\pi^2}{2L} + M_{Yb}W_{ma}\varnothing_{ma}\dfrac{2}{L} - \left(\varnothing_{ma} - \varnothing_{m,ini}\right)F_x\dfrac{\pi^2}{2L} \end{bmatrix} \tag{61}$$

The equation system can be solved analytically. The resulting displacement increments are as follows:

$$\Delta W_m = \frac{-M_{Yb}\dfrac{\pi^2}{8F_y}\left[\dfrac{M_{cr}^{\ 2}}{M_{Yb}^{\ 2}} - 1\right] - V_{m,ini}\varnothing_{ma}\dfrac{\pi^2 F_z}{32F_y} + \varnothing_{m,ini}\varnothing_{ma}\dfrac{M_{cr}^2}{M_{Yb}}\dfrac{\pi^2}{32F_y}}{\dfrac{M_{cr}^{\ 2}}{M_{Yb}^{\ 2}} - 1 + \varnothing_{ma}^2\dfrac{F_z}{8F_y}} - W_{ma} \tag{62}$$

$$\Delta V_m = \frac{V_{m,ini}\dfrac{M_{cr}^{\ 2}}{M_{Yb}^{\ 2}} + V_{m,ini}\varnothing_{ma}^2\dfrac{F_z}{8F_y} + \varnothing_{ma}\dfrac{M_{Yb}}{2F_y} - \varnothing_{m,ini}\dfrac{F_x}{M_{yb}}}{\dfrac{M_{cr}^{\ 2}}{M_{Yb}^{\ 2}} - 1 + \varnothing_{ma}^2\dfrac{F_z}{8F_y}} - V_{ma} \tag{63}$$

$$\Delta \varnothing_m = \frac{-V_{m,ini}\dfrac{F_z}{M_{Yb}} - \varnothing_{ma}\dfrac{F_z}{2F_y} + \varnothing_{m,ini}\dfrac{M_{cr}^{\ 2}}{M_{Yb}^{\ 2}}}{\dfrac{M_{cr}^{\ 2}}{M_{Yb}^{\ 2}} - 1 + \varnothing_{ma}^2\dfrac{F_z}{8F_y}} - \varnothing_{ma} \tag{64}$$

The expressions for the displacement can slightly be simplified if the initial shape is the buckling shape, i.e., when the initial twist and initial lateral translation are dependent on each other. However, whether the initial shape is the buckling shape or not, it is clear that the lateral translation and twisting rotation are different from those predicted by the Young's formula. Moreover, the formulae for V and $\varnothing$ are different.

An important characteristic of these formulae is that if the sign of the initial geometry is reversed then (i) the vertical W displacement is unchanged, (ii) the sign of the lateral increment is reversed, and (iii) the sign of the twisting rotation increment is reversed. This also means that a symmetric bifurcation is predicted (as the initial displacement converges to zero).

As the bending moment increases, the denominator of the formulae can decrease to zero, which identifies singularity. From the formulae it can be seen that the singularity belongs to a bending moment smaller than M_{cr}. The distance of the singularity to M_{cr} is largely dependent on the twisting rotation (squared). Since the whole analytical model is based on the assumption that the displacements are small, the bending moment where singularity happens is only marginally smaller than M_{cr}.

Another theoretical observation is that the primary (W) and secondary (V and $\varnothing$) displacements are not independent. However, the secondary ones are not affected by the primary one, only the primary one is affected by the secondary ones. This influence is typically small, again, because the displacements themselves are (or: assumed to be) small.

7 Comparison to shell FEM: stresses

Three members are considered. All are simply supported and subjected to uniform major-axis bending, and all have doubly-symmetric I-shaped sections. The depth of each section is 200 mm, the flange and web thicknesses are 20 mm. One cross-section has a flange width of 50 mm (referred to as *narrow I-section*), another has a flange width of 200 mm (referred to as *wide I-section*), while the third one has a flange width of 100 mm (referred to as *medium I-section*). The member length is either 2 or 4 m. Standard isotropic steel material is used, $E = 210$ GPa, $G = 80.8$ GPa. GNI analyses are performed, and stresses are calculated by using the new formulae, as well as by shell FEM.

For the shell FEM calculations, the Academic Teaching Introductory Release of the commercial Ansys software [18] is employed. The beams are modelled by shell elements, by using the so-called SHELL181 element, which is a four-node element with six degrees of freedom at each node (3 translations + 3 rotations). The element is based on the first-order shear-deformation theory (usually referred to as Mindlin-Reissner shell theory). It has large deflection and large strain capabilities.

The finite element mesh is highly regular. The maximum element size in the transverse direction was set to 20 mm (which means, e.g., 10 elements along the web depth). In the longitudinal direction the element size is larger (in order to decrease the total number of elements), however, it was defined so that the aspect ratio would not be too large.

The end support conditions are modelled using kinematic coupling constraints which relate the displacements of the cross-section nodes to a master node at the first and last cross-sections. The master node is defined at the mass center of the cross-section. The transverse translational displacement degrees of freedom are included in the coupling, in order to allow the end-section to warp freely. To model the fork supports, the master nodes are supported against transverse translation and against twisting (plus at one end the longitudinal translation is supported, too, in order to avoid potential numerical instabilities).

It is to underline that the cross-section stress (according to beam model theory) is the superposition of three components: major-axis bending, minor-axis bending, and warping torsion, as illustrated in Fig. 5.

In our study the major-axis bending is the primary stress, while the other two components are the secondary stresses, due to the developed lateral translation and twisting rotation (which are due to the initial geometric imperfection). The stresses at the flange tips, therefore, can be interpreted/calculated by the generic formula:

$$\sigma_{x,ABCD} = \pm\sigma_{x,major} \pm \sigma_{x,minor} \pm \sigma_{x,warping}. \tag{65}$$

In order to better separate the effect of initial lateral translation and initial twisting rotation, only one of these two imperfection components is considered in this specific analyses. The longitudinal normal stresses are calculated at various load levels for the middle cross-section, selected results are summarized in Tables 1 and 2. (The stress values in the Tables belong to a load level $M_Y/M_{cr} = 0.55$.)

It is obvious that the secondary stresses are generally non-negligible, they can be quite significant, they can even be larger than the stresses from the primary loading. The magnitude of the secondary stresses is proportional to the magnitude of the V and $\varnothing$ displacements. Consequently, the influence of the secondary stresses is proportional to the magnitude of V and $\varnothing$ displacements, which is primarily determined by (i) the initial magnitude of the geometric imperfection, (ii) the cross-section shape, and (iii) the member length, as can be concluded from Eqs. (62–64). Practically: secondary stresses are larger if the initial imperfection is larger, and if the flanges are wider, and if the member is shorter.

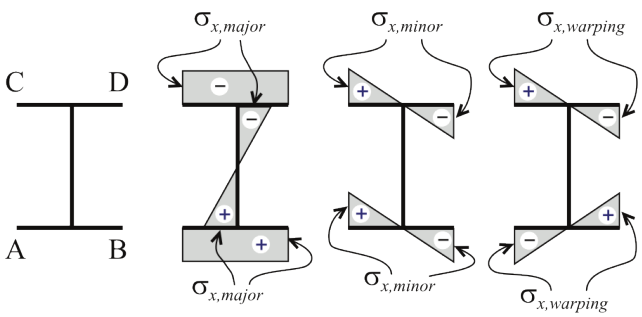

Fig. 5 Components of longitudinal normal stresses

It is also noteworthy to mention that stresses from shell FEM cannot be considered as perfect. It is well-known that the calculated stresses at the boundaries of the finite elements are extrapolated, the stresses are not-compatible at the element edges, that is why some kind of smoothing/averaging is usually applied in FEM softwares. Hence, stress calculation from a shell FE model requires approximations and engineering judgments.

It is also to mention that at higher load levels the shell FEM stresses themselves show certain inconsistency in the sense that they cannot exactly be superposed from the 3 linear components. This is the sign of the fact that a shell model is never identical to a beam model, e.g., the cross-sections do not remain perfectly rigid, the stress field is more general than the one assumed by beam models, etc.

Table 1 Stresses at the flange tips from GNIA with lateral imperfection

	cross-section point	shell FEM (MPa)	New analyt. model (MPa)
b = 200 mm	A	1153	1149
L = 2 m	B	1131	1118
V_0 = L/1000	C	-1212	-1233
$\varnothing_0 = 0$	D	-1055	-1035
b = 200 mm	A	1198	1212
L = 2 m	B	1086	1055
V_0 = L/200	C	-1528	-1629
$\varnothing_0 = 0$	D	-741	-638
b = 100 mm	A	201.3	201.0
L = 4 m	B	213.2	213.8
V_0 = L/1000	C	-223.3	-222.8
$\varnothing_0 = 0$	D	-190.9	-192.0
b = 100 mm	A	177.8	175.4
L = 4 m	B	236.4	239.4
V_0 = L/200	C	-287.3	-284.4
$\varnothing_0 = 0$	D	-126.7	-130.4
b = 50 mm	A	224.0	220.7
L = 2 m	B	236.5	234.4
V_0 = L/1000	C	-246.6	-242.7
$\varnothing_0 = 0$	D	-213.7	-212.4
b = 50 mm	A	199.4	193.4
L = 2 m	B	261.2	261.7
V_0 = L/200	C	-311.8	-303.5
$\varnothing_0$	D	-148.4	-151.6

Table 2 Stresses at the flange tips from GNIA with twist imperfection

	cross-section point	shell FEM (MPa)	New analyt. model (MPa)
b = 200 mm	A	1214	1198
L = 2 m	B	1070	1069
V_0 = L/1000	C	-1004	-986
$\varnothing_0 \times h/2 = L/1000$	D	-1264	-1282
b = 200 mm	A	1285	1263
L = 2 m	B	997	1005
V_0 = L/200	C	-874	-838
$\varnothing_0 \times h/2 = L/500$	D	-1392	-1430
b = 100 mm	A	282.8	286.3
L = 4 m	B	130.6	128.5
V_0 = L/1000	C	-109.7	-106.7
$\varnothing_0 \times h/2 = L/1000$	D	-303.4	-308.1
b = 100 mm	A	355.2	365.2
L = 4 m	B	54.8	49.6
V_0 = L/200	C	-14.0	-6.0
$\varnothing_0 \times h/2 = L/500$	D	-395.8	-408.8
b = 50 mm	A	314.7	314.5
L = 2 m	B	145.6	140.6
V_0 = L/1000	C	-121.9	-118.6
$\varnothing_0 \times h/2 = L/1000$	D	-338.1	-336.5
b = 50 mm	A	398.0	401.5
L = 2 m	B	61.9	53.7
V_0 = L/200	C	-14.8	-9.6
$\varnothing_0 \times h/2 = L/500$	D	-444.3	-445.5

By considering all these aspects, it is fair to say that the shell FEM results and the results from the new analytical model show good agreement, at least until the V and $\varnothing$ displacements remain small.

8 Comparison to shell FEM: load-displacement paths

In this section the member length is 2 m, and the wide and narrow cross-sections are discussed. The imperfection is taken as the buckling shape, the initial value of the lateral translation was set to 2 mm, which is 1/1000 of the length. Otherwise, the analyses are identical to those in the previous section.

Now the focus is on the load-displacement path. Selected results are presented in Figs. 6–8. The plots demonstrate that the second-order lateral translation and twisting rotation are smaller than what the Young-formula predicts. The deviation increases as the moment increases. It can also be observed that: the wider the flanges are, the larger the deviation from the Young-prediction is. Though the vertical, primary displacement is slightly different from the first-order solution (which is a straight line in the load-displacement plot), the deviation from the first-order solution is rather small.

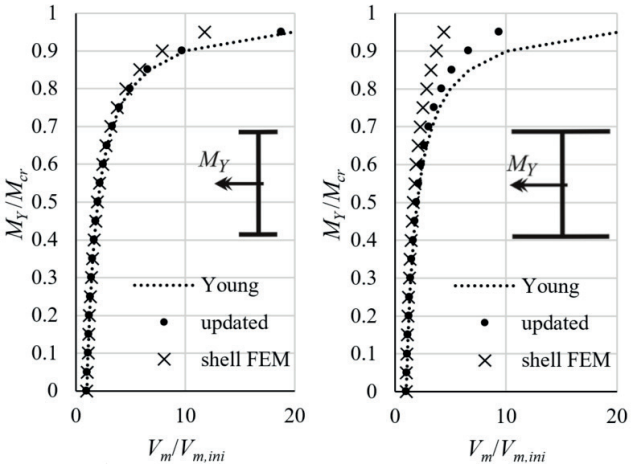

Fig. 6 Load vs. lateral translation

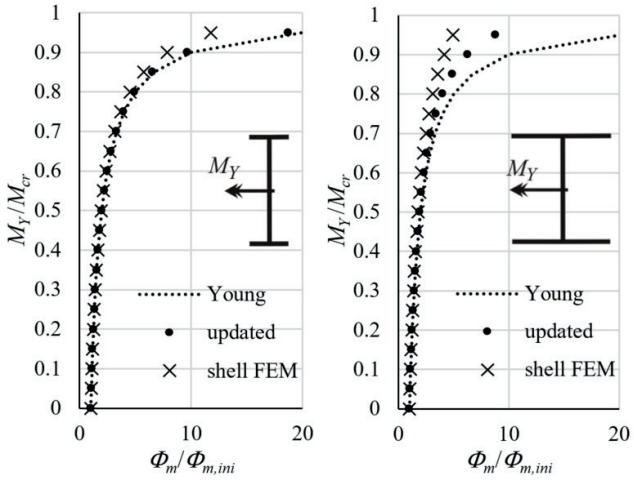

Fig. 7 Load vs. twisting rotation

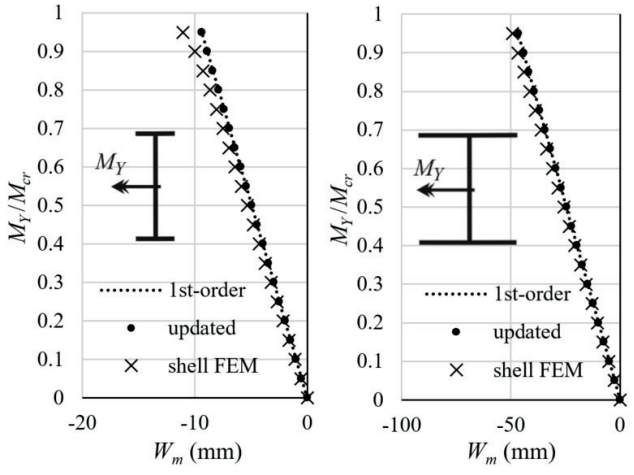

Fig. 8 Load vs. vertical translation

A general observation is that the actual values from the presented analytical solution and from the shell FEM are not identical. It is important to understand that exact agreement cannot be expected due to the differences between the two models. One difference is that in the shell FE model the longitudinal distribution of the displacements can slightly be different from those assumed in the analytical model. Also, there are deformations in the shell model which are neglected in the analytical model: in-plane shear deformations, small localized plate bending deformations, and also out-of-plane shear deformations (since the SHELL181 finite element of Ansys is based on the Reissner-Mindlin plate theory). The differences between the analytical and shell FEM results are not limited to the secondary displacements, but differences are experienced in the critical moments as well as in the primary displacements (see Fig. 7). Still, it is clear that the tendencies how and when the load-displacements paths deviate from the classic analytical solutions (e.g., Young's formula) are the same from both the newly introduced analytical model and from the shell FEM calculations.

9 Conclusions

In this paper new, updated analytical solutions were shown for the GNI analysis of simple beams subjected to lateral-torsional displacements. Closed-form formulae were derived to follow the non-linear second-order load displacement path of an initially imperfects beam. Numerical studies were performed to compare the results from the new formulae and those from shell finite element calculations. The new analytical formulae predict symmetric bifurcation for doubly-symmetric cross-section, just as classic analytical solutions. However, the secondary displacements are smaller than those calculated from Young's formula, and the difference is getting larger as the flange width increases. Moreover, the influence of the secondary displacements on the primary ones is clearly visible. The results show that the derived new formulae are able to capture the behavior predicted by shell finite element analysis. Even though there are numerical differences, the tendencies are similar. The new analytical solutions well explain the differences between the results of classic analytical solutions and shell finite element analyses. Based on the presented derivations and numerical results, it is clear that the key question is whether the secondary stresses due to the lateral translation and twisting rotation are considered or not during the analysis: classic analytical solutions do not consider this factor (therefore the stiffness is assumed to be independent of the actual deflections of the member), while standard finite element procedures do consider this factor (therefore the stiffness of the member is updated).

The primary importance of the presented research is that it proves analytically that classic analytical solutions for the lateral-torsional behavior of imperfect beams are necessarily different from solutions that apply an incremental procedure with stiffness updating. Moreover, the derivations clearly highlight the reason of the differences.

From practical aspect, the results suggest that the nonlinear behavior is influenced by the geometrical proportions of the cross-section: the wider the flanges are, the farther the behavior is from the one predicted by the Young's formula. This dependency of the nonlinear behavior on the cross-section proportions indicates that the LTB capacity of the beam – among other factors, such as residual stresses – is dependent on the cross-section geometry.

Though it would be unfair to suggest that classic analytical solutions are incorrect, still, it is fair to say that a calculation method with stiffness updating is a better description of the physical reality, therefore carefulness is needed when classic analytical solutions are applied.

Acknowledgement

The presented work was conducted with the financial support of the K138615 project of the Hungarian National Research, Development and Innovation Office.

References

[1] Timoshenko, S. P., Gere, J. M. "Theory of Elastic Stability", McGraw-Hill, 1961. ISBN-10 0078582172

[2] Vlasov, V. Z. "Thin-walled elastic beams", National Science Foundation, Washington, D.C. (by the Israel Program for Scientific Translations) [translated from Russian by Y. Schectman, original title: Tonkostennye uprugie sterzhni]

[3] Trahair, N. S. "Flexural-Torsional Buckling of Structures", Chapman and Hall, 1993. ISBN 9780367449834

[4] Melcher, J. "Kippen von Tragern als Stabilitatsproblem zweier Gruppen von Querschnittypen (Lateral beam buckling as a stability problem of two groups of cross-section types)", Stahlbau, 68(1), pp. 24–29, 1999. https://doi.org/10.1002/stab.199900060

[5] Balázs, I., Melcher, J., Horacek, M., Pesek, O. "On Problem of Efficient Determination of Elastic Critical Moment of Beams with Selected Types of Cross-Sections", IOP Conference Series: Materials Science and Engineering, 471, 052041, 2019. https://doi.org/10.1088/1757-899X/471/5/052041

[6] Glauz, R. S. "Elastic lateral-torsional buckling of general cold-formed steel beams under uniform moment", Thin-Walled Structures, 119, pp. 586–592, 2017. https://doi.org/10.1016/j.tws.2017.07.010

[7] Hoang, T., Ádány, S. "Torsional Buckling of Thin-Walled Columns with Transverse Stiffeners: Analytical Studies", Periodica Polytechnica Civil Engineering, 64(2), pp. 370–386, 2020. https://doi.org/10.3311/PPci.15137

[8] Young, T. "A course of lectures on natural philosophy and the mechanical arts", Royal Institution of Great Britain, 1807.

[9] Ayrton, W. E., Perry, J. "On struts", The Engineer, 62, 1886.

[10] Maquoi, R., Rondal, J. "Mise en Equation des Nouvelles Courbes Européennes de Flambement" (Equation for the New European Buckling Curves), Construction Métallique, 15(1), pp. 17–30, 1978.

[11] CEN "EN 1993-1-1:2005, Eurocode 3, Design of Steel Structures, Part 1-3: General rules and rules for buildings", European Committee for Standardization, Brussels, Belgium, 2005.

[12] CEN "EN 1993-1-3:2006, Eurocode 3, Design of Steel Structures, Part 1-3: General rules, Supplementary rules for cold-formed members and sheeting", European Committee for Standardization, Brussels, Belgium, 2006.

[13] Szalai, J., Papp, F. "On the theoretical background of the generalization of Ayrton-Perry type resistance formulas", Journal of Constructional Steel Research, 66, pp. 670–679, 2010. https://doi.org/10.1016/j.jcsr.2009.12.013

[14] Agüero, A, Pallarés, F. J., Pallarés, L. "Equivalent geometric imperfection definition in steel structures sensitive to lateral torsional buckling due to bending moment", Engineering Structures, 96, pp. 41–55, 2015. https://doi.org/10.1016/j.engstruct.2015.03.066

[15] Haffar, M. Z., Taher, M. H., Ádány, S. "On the GNI analysis of simple thin-walled beams with using linear buckling mode as geometric imperfection", In: Proceedings of the International Colloquium on Stability and Ductility of Steel Structures, Prague, Czech Republic, 2019, pp. 468–475. ISBN 9780429320248

[16] Kala, Z. "Elastic lateral-torsional buckling of simply supported hot-rolled steel I-beams with random imperfections", Procedia Engineering, 57, pp. 504–514, 2013.

[17] Haffar, M. Z., Ádány, S. "Analytical solutions for the GNI analysis for lateral-torsional buckling of thin-walled beams with doubly-symmetric and mono-symmetric cross-sections", In: Proceedings of the 8th International Conference on Coupled Instabilities in Metal Structures (CIMS 2021), Lodz, Poland, 2021, pp. 1–8. https://doi.org/10.2139/ssrn.3868235

[18] Ansys Inc. "Ansys Release 2020 R1" [online] Available at: https://www.ansys.com/blog/ansys-2020-r1